Aging in a Laponite colloidal suspension: A Brownian dynamics simulation study

S. Mossa
European Synchrotron Radiation Facility, B.P. 220, F-38043 Grenoble, France

C. De Michele and F. Sciortino
Dipartimento di Fisica, Università di Roma "La Sapienza," Piazzale A. Moro 2, I-00185, Roma, Italy; INFM Udr, Via Marzolo 8, 35131 Padova, Italy; and SOFT: Complex Dynamics in Structured Systems, Università di Roma "La Sapienza," Piazzale A. Moro 2, I-00185, Roma, Italy

(Received 20 July 2006; accepted 17 November 2006; published online 4 January 2007)

The authors report Brownian dynamics simulation of the out-of-equilibrium dynamics (aging) in a colloidal suspension composed of rigid charged disks, one possible model for Laponite, a synthetic clay deeply investigated in the last few years by means of various experimental techniques. At variance with previous numerical investigations, mainly focusing on static structure and equilibrium dynamics, the authors explore the out-of-equilibrium aging dynamics. They analyze the wave vector and waiting time dependence of the dynamics, focusing on the single-particle and collective density fluctuations (intermediate scattering functions), the mean-squared displacement, and the rotational dynamics. Their findings confirm the complexity of the out-of-equilibrium dynamical behavior of this class of colloidal suspensions and suggest that an arrested disordered state driven by a repulsive Yukawa potential, i.e., a Wigner glass, can be observed in this model. © *2007 American Institute of Physics*. [DOI: 10.1063/1.2408418]

I. INTRODUCTION

The out-of-equilibrium dynamical behavior of soft matter—and gels, in particular—still constitutes an interesting puzzle in condensed matter physics.[1–3] Indeed, despite the fact that out-of-equilibrium nonergodic soft materials are ubiquitous in the everyday life, the mechanisms governing their dynamics are still unclear. An adequate comprehension of the above mechanisms is important for at least two main general reasons. First, particles ranging from about 10 nm to microns are currently used as building blocks of nanostructured composite materials, therefore having strong implications in industrial processing and technology development. Second, soft matter systems can help with fundamental questions about the nature of condensed matter. Indeed, due to the fact that interactions can be chemically tuned (strength, range) with a high degree of accuracy, they can provide a good implementation of particular limits as, for instance, the hard sphere purely repulsive potential, and can be used to test most of the theoretical models developed to address the physics of liquids.

From an experimental point of view, relevant time and length scales in colloidal systems are more easily accessible than in the case of simple atomic and molecular supercooled liquids and glasses.[4] Nowadays dynamics can be studied to relatively long time scales, and average collective dynamics is accessible together with single-particle behavior. Different spectroscopies are commonly used, ranging from light and x-ray scattering to confocal microscopy.[2,5,6] These techniques allow one to access the instantaneous state of the system not only under the form of spectra or correlation functions of the observables of interest, but also as direct snapshots (configurations) of the system. The direct knowledge of the space position of the particles can be directly used to calculate all the relevant quantities or also for visual inspection,[7] sometimes giving a direct physical intuition of the mechanisms controlling the dynamics.

While technological improvement has strongly developed the above experimental scattering techniques, theoretical descriptions often lay behind, due to difficulties in modeling the interparticle potentials and in providing a proper description of the role of the solvent. Indeed, properties of colloidal systems have often been studied by classical Newtonian molecular dynamics simulations, where the interaction among particles (either spherical or anisotropic) are schematized by simple isotropic potentials. The above approach completely neglects the interaction of the colloidal particles with the solvent where they are dispersed, not to mention hydrodynamic effects. Important steps have been made in the direction of more realistic descriptions implementing lattice Boltzmann and fluid particle dynamics methods, where hydrodynamic effects are also considered.[8–10] These approaches are very demanding from a computational point of view, strongly limiting both the size of the considered systems and the time and length scales accessible by the simulation. An intermediate approach is provided by Brownian dynamics simulation (i.e., neglecting hydrodynamic interactions) by correctly taking into account the interaction of a possibly anisotropic colloidal particle with the solvent and in the presence of a more realistic interaction potential among the constituents. This intermediate approach, being computationally feasible, could help in understanding out-of-equilibrium dynamics on very long time scales.

In this work we introduce a new Brownian dynamics

algorithm and study the out-of-equilibrium dynamics of a colloidal suspension formed by strongly anisotropic discoticlike particles, which is believed to be a good model for *Laponite*. Laponite is an interesting material; it is a synthetic clay, deeply investigated in the last few years by means of several experimental techniques.[11–17] This system presents many different open problems, ranging from the correct description of the phase diagram[17–22] to the out-of-equilibrium and aging dynamics,[23–25] also under particular external conditions.[26] Previous computer simulations have focused on the static structure and the role played by the distribution of the charges on the platelet.[27–29] A Brownian dynamics simulation has been presented in Ref. 30, with a focus on structure and dynamics at equilibrium. Here we present an analysis of the out-of-equilibrium dynamics of a model introduced in Ref. 27, where a Laponite platelet is modeled by identical negatively charged interacting sites, uniformly distributed in a two-dimensional disklike geometry.

The paper is organized as follows. Section II contains an overview of the experimental phase diagram of Laponite and a description of experiments pointing to the existence of an ergodic to nonergodic phase transition. Section III is a description of the model we have used to describe the interaction between two Laponite platelets, while in Sec. IV we briefly recall the principles of Brownian dynamics and introduce our algorithm for the integration of the equations of motion in the case of strongly anisotropic colloidal particles. Section V reports the details of the computer simulations. The next four sections contain a detailed investigation of the long-time aging dynamics of the model. Section VI reports a study of the mean-squared displacement of the particles; the one-particle and collective dynamics of density fluctuations are included in Sec. VII and VIII, respectively. Section IX concludes the study of the out-of-equilibrium dynamics with the rotational dynamics behavior of the system. Finally, Sec. X contains a discussion of our main results and the conclusions.

II. LAPONITE

Laponite is a very interesting material. Not only is it used in several industrial processes, but it has also been widely investigated by means of the most powerful experimental techniques. It is a synthetic clay, formed by very thin cylindrical platelets of radius $r_0 \simeq 12.5$ nm and thickness $d_0 \simeq 1$ nm. The total uniform surface charge is $Q \simeq Ze$, with $Z \simeq -700$. Laponite phase diagram has been investigated in detail in Ref. 18. Recently significant modifications to the phase diagram of Ref. 18 have been proposed by different authors.[17,19–21]

In a series of papers,[11–14] dynamic arrest in Laponite has been interpreted as formation of a *Wigner glass*. In particular, aging of a glass is related to the presence of cages of particles at high concentration, mainly due to repulsive interactions, while gelation corresponds to cluster formation due to attraction. Recently Ruzicka *et al.*[19–21] have performed dynamic light scattering experiments to study aging and structural arrest for both low and high concentrations. Measurements performed over long periods of time have shown two different routes to arrest, depending on the role of attractive short-ranged interactions. The situation is reminiscent of the case where competing interactions are present, which gives rise to Wigner-type glasses.[31,32]

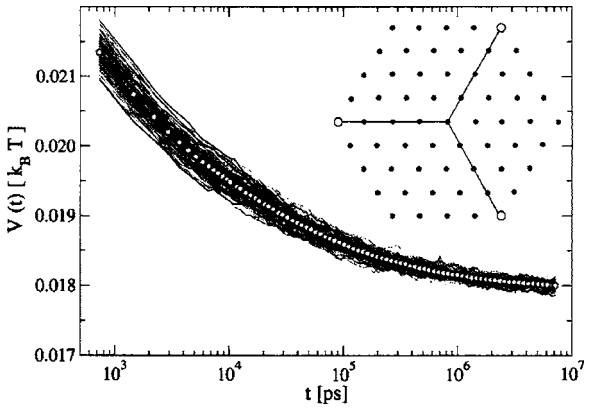

FIG. 1. Main panel: Relaxation of potential energy as a function of time after the temperature jump. 100 independent realizations of the system have been equilibrated at high temperature, $T=500$ K, and at $t_w=0$, instantaneously quenched to $T=300$ K. In the plot we show the data for each run (lines) and the averaged value (symbols). Note that the energy stays positive due to the purely repulsive nature of the interaction site-site potential. The relaxation of the energy follows a power law behavior of exponent $\gamma \simeq 0.35$ and the value predicted at equilibrium (estimated at $E_\infty \simeq 0.0178 k_B T$) is not reached on the total simulation time scale. Therefore, the systems stay out of equilibrium for the total duration of the present simulation. Inset: Hexagonal grid with $\nu=61$ charge sites used as a model for a Laponite platelet. The open circles identify the three dynamical sites.

A different interpretation has been proposed by Nicolai and co-workers[15–17] based on a picture in which aggregation between the platelets is induced by salt addition, which reduces electrostatic repulsion and produces fractal aggregates that will eventually form a gel. It was suggested that attractive interaction leads to aggregation of the Laponite particles and the formation of a *house of cards* structure. It was recently shown that the presence of positive charges on the rim of the Laponite disks is necessary to induce aggregation and gelation.[17,33] These charges were neutralized by added pyrophosphate, and aggregation and gelation were slowed down, even though the resulting ionic strength was increased.

III. THE INTERACTION MODEL

We consider here the interaction model introduced in Ref. 27 and conventionally named *model A*, where the total negative charge is uniformly distributed over the surface area and the possible presence of positive rim charges is neglected. In this respect, this work constitutes an effort in the direction of quantifying the routes to dynamic arrest driven by repulsive interactions which progressively establishes via structural reorganization of the system. Future work must address the issue of the differences in arrest introduced by the presence of attractions mediated by oppositely charged rim particles.[34]

Following the authors of Ref. 27, each Laponite platelet is schematized as a rigid disk, formed by $\nu=61$ charge sites disposed on a regular mesh with grid points spaced by $r_0/4$ (see Fig. 1). Each site carries a charge $q=Q/\nu \simeq -11.47e$.

The solvent (water in the present case) is treated as a continuum of dielectric constant $\epsilon=78$.

The position of the platelet can be determined by the three coordinates of its center of mass and the three Euler angles or, equivalently, by the coordinates of a subset of points sufficient to define the molecular geometry.[35] We choose the latter description and consider three dynamics sites (open circles in the inset of Fig. 1), i.e., the ones whose dynamics is explicitly integrated in time to generate the Brownian molecular dynamics trajectory. The dynamical sites have mass $m=747\,900m_p$ (here m_p is the mass of the proton), are placed at the vertices of an equilateral triangle of side $\sqrt{3}r_0$, and their center of mass coincides with the center of mass of the entire platelet. Note that the choice of the dynamical sites is arbitrary (the only requirement being that they are noncollinear), and the actual choice we made is merely due to symmetry considerations. (In the present case, we obviously do not expect the moments of inertia of a homogeneous Laponite platelet to be exactly reproduced by a trimmer. This notwithstanding, we are convinced that our choice is a rather good approximation and has no large consequences on the dynamics.)

The remaining interaction sites are massless, their positions can be directly calculated at any time in terms of the coordinates of the dynamical sites, and they are taken into account only in the calculation of the constraint forces acting on the dynamical sites. Therefore, for each dynamical site we correctly take into account both the intermolecular forces and the intramolecular contributions coming from the secondary sites.

The total interaction energy between two platelets is the sum of ν^2 site-site screened Coulomb electrostatic interactions of the Yukawa form. The interaction between sites k and l at positions $\mathbf{r}_k$ and $\mathbf{r}_l$ and pertaining to two different platelets is therefore of the form[4,27,36]

$$V_{kl}=\frac{q_k q_l e^2}{\epsilon}\frac{e^{-r_{kl}/\lambda_D}}{r_{kl}}, \tag{1}$$

where $r_{kl}=\|\mathbf{r}_k-\mathbf{r}_l\|$ and λ_D is the Debye screening length of the microions, i.e.,

$$\lambda_D=\sqrt{\frac{\epsilon k_B T}{4\pi(n_+ z_+^2+n_- z_-^2)e^2}}. \tag{2}$$

In the above equation, (n_+,z_+) and (n_-,z_-) are the concentrations and the valences of positive counterions and negative coions coming from the platelets and the salt added to the solution.

IV. BROWNIAN DYNAMICS AND THE INTEGRATION ALGORITHM

In this article we introduce a novel algorithm to integrate the Brownian equations of motion which, although neglecting hydrodynamics effects, takes into account the presence of the solvent in the dynamics. Most Brownian dynamics simulations are based on the original Ermak algorithm[37] developed for atomic systems, where the friction coefficient associated with the damping force and acting on spherical objects is isotropic. The Ermak algorithm has been generalized by van Gunsteren and Berendsen[38] to the case of molecules formed by spherical centers of interaction, for which the choice of an isotropic friction coefficient is still appropriate. In contrast, in the present case of a strongly anisotropic rigid particle, one should take into account the fact that the platelet moves differently in the directions perpendicular and parallel to its symmetry axis.

To the best of our knowledge, the only other attempt to take into account in a reasonable fashion the anisotropy of a discoticlike particle in a Brownian dynamics computer simulation has been the one by Odriozola *et al.*,[30] based on the integration of the Langevin equations of a rigid body, separately for the center of mass and for the orientation. In the present work we prefer to rely on the original work by Ermak, which allows us to find an optimal balance between a reasonable realism of the molecular model and an acceptable efficiency. This gives us the possibility to follow the dynamics of the system on time scales much longer than the ones investigated so far.

In our algorithm the viscous damping and the Brownian forces act on each of the three sites with mass but the friction coefficient ξ is chosen different in the directions perpendicular ($\xi_\perp$) and parallel ($\xi_\parallel$) to the symmetry axis of the platelet, which we choose parallel to the normal to the surface. The numerical values of the two friction coefficients must be chosen properly, in order to reproduce a realistic dynamics for the free diffusion of the single platelet, as we will describe in detail in Sec. V. $\xi_\perp$ and $\xi_\parallel$ are used to evaluate the following numerical coefficients:

$$c_0^\alpha=e^{-\xi_\alpha\delta t},\quad c_1^\alpha=\frac{1-c_0^\alpha}{\xi_\alpha\delta t},\quad c_2^\alpha=\frac{1-c_1^\alpha}{\xi_\alpha\delta t}, \tag{3a}$$

$$(\sigma_r^\alpha)^2=\frac{k_B T}{m}\frac{\delta t}{\xi_\alpha}\left(2-\frac{3-4e^{-\xi_\alpha\delta t}+e^{-2\xi_\alpha\delta t}}{\xi_\alpha\delta t}\right),$$

$$(\sigma_v^\alpha)^2=\frac{k_B T}{m}(1-e^{-2\xi_\alpha\delta t}), \tag{3b}$$

$$c_{rv}^\alpha=\frac{k_B T}{m}\frac{1}{\xi_\alpha\sigma_r^\alpha\sigma_v^\alpha}(1-e^{-\xi_\alpha\delta t})^2, \tag{3c}$$

where $\alpha=\perp,\parallel$ and δt is the integration time step.

For each dynamical site of mass m of the platelet, and at the time $(t+\delta t)$, the integration algorithm can be schematized as follows:

(1) Each pair of components of the vectors

$$\delta\mathbf{r}=(\delta r_x,\delta r_y,\delta r_z), \tag{4a}$$

$$\delta\mathbf{v}=(\delta v_x,\delta v_y,\delta v_z), \tag{4b}$$

is sampled from a bivariate Gaussian distribution with zero mean values, variances given by $(\sigma_r^\alpha)^2$ and $(\sigma_v^\alpha)^2$ [Eq. (3b)], and a correlation coefficient determined by c_{rv}^α [Eq. (3c)] (see Ref. 39). With this step we produce a realization of the stochastic process appropriate to generate Brownian motion.

(2) Transform position $\mathbf{r}(t)$, velocity $\mathbf{v}(t)$, and forces $\mathbf{F}(t)$ evaluated in the laboratory-fixed frame at time t to $\mathbf{r}'(t)=(r'_x,r'_y,r'_z)$, $\mathbf{v}'(t)=(v'_x,v'_y,v'_z)$, and $\mathbf{F}'=(F'_x,F'_y,F'_z)$ in the body (platelet)-fixed reference frame, where the z axis is chosen parallel to the platelet symmetry axis

$$\mathbf{r}'(t) = \mathbf{R}(t)\mathbf{r}(t), \tag{5a}$$

$$\mathbf{v}'(t) = \mathbf{R}(t)\mathbf{v}(t), \tag{5b}$$

$$\mathbf{F}'(t) = \mathbf{R}(t)\mathbf{F}(t); \tag{5c}$$

here $\mathbf{R}(t)$ is the appropriate orthogonal matrix corresponding to the change of the reference frame (evaluated at time t).

(3) Update positions in the body-fixed reference frame to $(t+\delta t)$ and velocities to $(t+\delta t/2)$, according to Ermak's prescription:

$$r'_\beta(t+\delta t) = r'_\beta(t) + c_0^\alpha v'_\beta \delta t + c_2^\alpha \frac{F'_\beta(t)}{m}\delta t^2 + \delta r_\beta, \tag{6a}$$

$$v'_\beta\left(t+\frac{\delta t}{2}\right) = c_0^\alpha v'_\beta(t) + (c_1^\alpha - c_2^\alpha)\frac{F'_\beta(t)}{m}\delta t + \delta v_\beta, \tag{6b}$$

where $\alpha=\parallel$ if $\beta=x,y$ and $\alpha=\perp$ if $\beta=z$. Note that $F'_\beta(t)$ are the forces evaluated at time t, acting onto the three sites carrying mass, transformed to the body-fixed reference frame. These forces include the intraplatelet contributions coming from the massless sites.

(4) Transform positions and velocities to the laboratory-fixed reference frame:

$$\mathbf{r}(t+\delta t) = \mathbf{R}^{-1}(t)\mathbf{r}'(t+\delta t), \tag{7a}$$

$$\mathbf{v}(t+\delta t) = \mathbf{R}^{-1}(t)\mathbf{v}'(t+\delta t). \tag{7b}$$

(5) Adjust positions and velocities using the RATTLE algorithm[39] in order to fulfill the rigid constraints (fixed distances) among the three sites with mass.

(6) Evaluate the forces $F_\beta(t+\delta t)$ acting on the site at time $(t+\delta t)$.

(7) Transform velocities $\mathbf{v}(t)$ and forces $\mathbf{F}(t)$ evaluated in the laboratory-fixed frame at time t to $\mathbf{v}(t)=(v'_x,v'_y,v'_z)$ and $\mathbf{F}'=(F'_x,F'_y,F'_z)$ in the body (platelet)-fixed reference frame using the orthogonal matrix $\mathbf{R}(t)$, as we did in step 2.

(8) Update velocities to $t+\delta t$ following Ermak's scheme:

$$v'_\beta(t+\delta t) = v'_\beta\left(t+\frac{\delta t}{2}\right) + c_2^\alpha \delta t \frac{F'_\beta(t+\delta t)}{m}, \tag{8}$$

where, again, $\alpha=\parallel$ if $\beta=x,y$ and $\alpha=\perp$ if $\beta=z$.

(9) Transform velocities back to the laboratory-fixed reference frame using the matrix $\mathbf{R}^{-1}(t)$, as we did in step 4.

(10) Finally, adjust velocities using the RATTLE algorithm to assure zero relative velocity among the dynamical sites.

V. SIMULATION DETAILS

We have simulated a system composed of $N=108$ Laponite platelets of radius $r_o=12.5$ nm. The time unit is $t_0=73.6$ ps and the time step used to integrate the equation of motions is $\delta t=0.1t_0$. The system is initially thermalized at a high temperature, $T=500$ K, and at time $t_w=0$, it is instantaneously quenched at room temperature, $T=300$ K. t_w is the *waiting time*, i.e., the elapsed time after the quench, and it is an additional relevant time scale for the dynamics of the system, as we will see below. The total volume of the system is $V=1.515\times10^6$ nm^3, which corresponds to a volume fraction $\phi=3.5\%$ in the case we assume that each platelet occupies a volume equal to $4\pi r_o^2 d_o=1963.5$ nm^3. We note that at a volume fraction $\phi=3.5\%$, corresponding to a weight concentration of about 9%, the experimental phase diagram of Laponite predicts a nematic phase.[40] In the model we study (with no rim charges), we do not find any buildup of nematic order in the system during the aging dynamics. The nematic order in the system has been checked, evaluating the nematic order parameter, defined as the largest eigenvalue of the ordering matrix.[41] This parameter is 0 for an isotropic system and 1 for a nematic one. We found that the nematic order parameter is always around 0.

The side length of the simulation box is $L=114.84$ nm and cubic periodic boundary conditions are used. The Debye screening length value chosen for the interaction potential Eq. (1) is $\lambda_D=3$ nm, a value which is believed to be appropriate for realistic experimental conditions.[27] The interaction potential is truncated when the distance between the two interacting sites exceeds a cutoff radius $r_c=10$ nm.

The numerical values of the friction coefficients, $\xi_\perp$ and $\xi_\parallel$, defined above have been chosen according to the following argument. A Laponite platelet can be assimilated to an oblate ellipsoid of semiaxes (a,b,c), with $a=b$ and $a>c$, which diffuses in a solvent (water) characterized by a viscosity η. In the case of an oblate ellipsoid, the translational diffusion coefficients, $D_\perp^T$ and $D_\parallel^T$—corresponding respectively to displacements perpendicular and parallel to the platelet surface—and the corresponding rotational diffusion coefficients, $D_\perp^R$ and $D_\parallel^R$—that correspond to rotations about axes perpendicular and parallel to the platelet surface, respectively—can be evaluated exactly (see, for instance, Ref. 42). More specifically, assuming that (i) we consider as a solvent pure water, i.e., $\eta=1.002$ cP; (ii) the freely diffusing oblate ellipsoid has an aspect ratio similar to that of the Laponite platelets, i.e., $a=12.5$ nm and $c=0.5$ nm; and (ii) the temperature is $T=300$ K; we have chosen the friction coefficients $\xi_\perp=0.016$ ps^{-1} and $\xi_\parallel=0.063$ ps^{-1}.

As we will see below, following the temperature jump, the simulated system does not reach equilibrium on the time scale of the simulation. This implies that two-time correlation functions will depend separately on the time difference t and the time t_w elapsed from the quench. Hence, average over starting times must be substituted with an average over an ensemble of several statistically independent initial configurations. We have considered 100 independent configurations of the systems, which have been equilibrated at high temperature $T=500$ K and, at time $t_w=0$, quenched instanta-

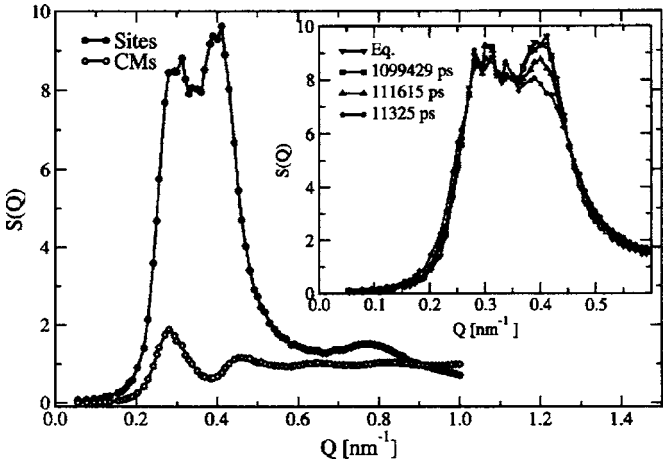

FIG. 2. Main panel: Equilibrium static structure factor $S(Q)$ calculated both for the platelet centers of mass (open circles) and interaction sites (closed circles). Each point is an average over 100 system configurations for $t > 10^6$ ps. The smallest value of Q accessible in our simulation is $Q_m = 2\pi/L \simeq 0.05$ nm^{-1}. For the wave-vector average, we have chosen a resolution $\Delta Q = 0.005$ nm^{-1} and up to 200 Q vectors have been considered for each value of Q. Error bars are smaller than the symbols. Inset: Variation of the static structure factor calculated on sites at short times at the indicated values of t. A slight change in the structure of the second subpeak is evident.

neously to ambient temperature $T=300$ K. We have calculated the Brownian dynamics trajectories for each sample for 10^6 integration time steps, corresponding to a total time interval of 7 μs. The total CPU time amounts to about 14 000 h on a farm of ten 2.6 GHz AMD Opteron CPUs. The evolution of the 100 independent systems has been recorded, and system configurations have been stored logarithmically spaced in time for the analysis presented in the following sections.

Following the temperature jump from high temperature, the energy of the system relaxes but never reaches thermodynamic equilibrium at the lower temperature. In Fig. 1 we show the energy relaxation for each sample (solid lines) and the average value (open circles). Note that, due to the repulsive nature of the interaction potential, the total potential energy is always positive. The relaxation follows a power law of exponent $\gamma \simeq 0.35$ and the equilibrium value (estimated at $E_\infty \simeq 0.0178 k_B T$) is not reached on the simulation time scale. Hence, the system is always out of equilibrium and explores a series of metastable states of lower and lower energy. In what follows we will characterize the aging dynamics and show that the slowing down of the dynamics strongly depends on the waiting time t_w.

In the main panel of Fig. 2 we show the static structure factor, $S(Q)=\langle \rho(Q)\rho^*(Q)\rangle$, where $\rho(Q)=(1/M)\Sigma_i^M \exp(i\mathbf{Q}\cdot\mathbf{X}_i)$ is the density fluctuation of wave vector $\mathbf{Q}$. Here and in the following, the coordinates $\mathbf{X}_i$ indicate either the center of mass of platelet $\mathbf{R}_i$ (in this case $M=N$) or the position $\mathbf{r}_i$ of all sites (in this case $M=61\times N$). The figure shows our results for both centers of mass (open symbols) and sites (closed symbols). In particular, latter data contain detailed informations on the form factor of the clay platelets and, therefore, they are the results most appropriate for a comparison with experimental measurements. We note, however, that the smallest wave-vector value accessible in our simulation has modulus $Q_m = 2\pi/L \simeq 0.055$ nm^{-1}, obviously far from the values typical of the most popular scattering techniques. Each point shown is a spherical average in momentum space with a resolution $\Delta Q = 0.05$ nm^{-1}, and up to 200 vectors have been considered for each value of Q. The data have been calculated from the configurations produced at times larger than 10^6 ps and no changes have been found in the static structure at later times. Only at much shorter times small changes are evident in the structure of the second subpeak for the case of interaction sites, as shown in the inset of Fig. 2.

In summary, from the above data it is evident that, following the temperature jump, the system starts to explore out-of-equilibrium states of lower and lower energy. During the above process the static structure does not significantly change at long times, as also found in the case of molecular glass formers. This is at strong variance with the long-time structural dynamics—as shown by the mean-squared displacement and density fluctuations correlation functions—which show spectacular changes, as we will report in the following sections.

VI. THE MEAN-SQUARED DISPLACEMENT

In this section we analyze the centers of mass mean-squared displacement of the center of mass of the platelets,

$$\langle r^2(t,t_w)\rangle = \frac{1}{N}\sum_{k=1}^{N} \langle |\mathbf{R}_k(t+t_w) - \mathbf{R}_k(t_w)|^2\rangle; \tag{9}$$

here $\langle\ \rangle$ is the average over the initial conditions. Note that in the calculations we have taken care of subtracting the displacement of the center of mass of the whole system, which does not vanish in Brownian simulations, to reveal the intrinsic dynamics of the particles. Indeed, in the case where the dynamics is very slow (as it is the case here), at long times the diffusion motion of the total center of mass can be relevant. In Fig. 3 we plot the mean-squared displacement at the indicated values of t_w. Following an initial transient regime, the curves reach a plateau, reminiscent of the cage effect in glassy systems, and whose lifetime increases on increasing t_w; only at later times, eventually, the curves move from the plateau and apparently bend toward a constant value. From these data we can tentatively argue that, for values of t_w longer than the one we can presently simulate, the system stops to flow on very long time scales and arrests in a disordered state.

The absence of a clear diffusive regime (even at long times) and the absence of equilibrium conditions do not allow us to extract from the mean-squared displacement data a diffusion coefficient via the Einstein relation. In order to identify a relevant time scale of the structural dynamics, without introducing any *ad hoc* model, we proceed as follows: we fix an arbitrary threshold value r^{2*}, and consider the time τ^* at which $r^2(\tau^*)=r^{2*}$. We repeat this analysis as a function of the waiting time t_w. In Fig. 4 (main panel) we show our results for several values of r^{2*}, ranging from 5 to 50 nm^2. The data have been rescaled by t_w and additionally shifted to maximize the overlap and stress the simple scaling with t_w which, therefore, seems to set the only rel-

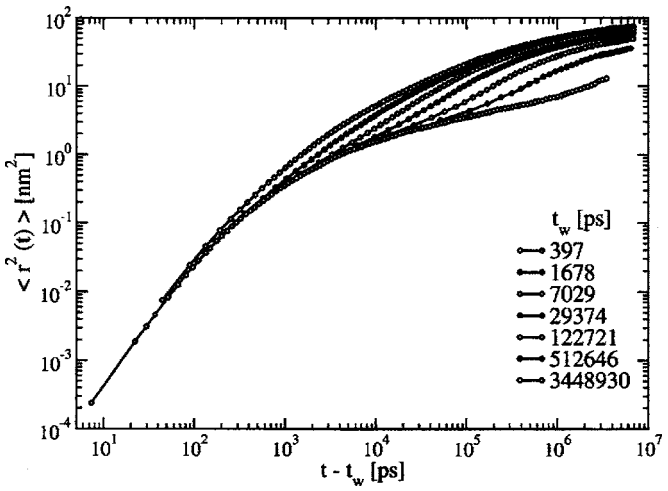

FIG. 3. Mean-squared displacement $\langle r^2(t,t_w)\rangle$, calculated for the platelet centers of mass, as discussed in the text, as a function of time for different waiting times t_w. Shorter waiting times are on the top. The initial transient dynamics at short t is followed by a plateau whose lifetime increases on increasing t_w. Next the curves move from the plateau, saturating to a (nearly) constant value at very long times. From these data we could argue that the system eventually stops to flow on very long time scales.

evant time scale for diffusion. In the inset of Fig. 4 we show the raw data for the case $r^{2*}=15$ nm^2. At short t_w the data can be represented by a function of the form $\tau^* \sim A+Bt_w^x$, with $x \simeq 0.64$. At longer t_w we observe the linear behavior $\tau^* \propto t_w$, expected for $\tau^* \simeq t_w$. Indeed, from simple models (see, for instance, Refs. 43 and 44), it is possible to show that the average lifetime of a potential energy landscape basin, trapping the system at a time of order t_w, cannot exceed t_w.

Already from these results it is clear that the aging dynamics forces us to introduce a new relevant time scale, t_w. This is of particular interest for the case of Q-dependent quantities, where we expect a particularly complex interplay between the length scales probed, the corresponding relaxation time τ_Q, and the waiting time t_w. In the following sections we therefore focus on the out-of-equilibrium dynamics of the density fluctuations.

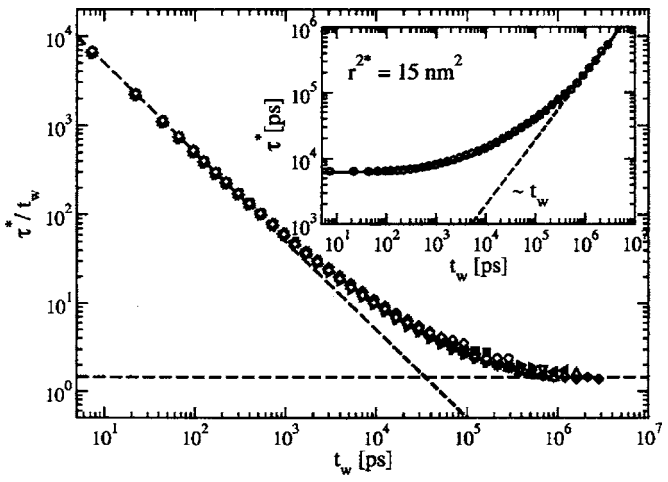

FIG. 4. Relevant dynamic time scale τ^* calculated from the mean-squared displacement, as discussed in the text. Main panel: τ^* as a function of t_w calculated for different values of r^{2*}, ranging from 5 to 50 nm^2. Data have been rescaled by t_w and additionally shifted to maximize the overlap and stress the simple scaling with t_w, which sets the relevant time scale. Inset: τ^* as a function of t_w for $r^{2*}=15$ nm^2. At short t_w data can be represented by a power law behavior, $\tau^* \simeq A+Bt_w^x$, with $x \simeq 0.64$ (solid line); at longer t_w, one observes the expected linear behavior $\tau^* \propto t_w$ (dashed line) (Ref. 50).

VII. ONE-PARTICLE DYNAMICS OF DENSITY FLUCTUATIONS

The relaxation dynamics of density fluctuations is encoded in the intermediate scattering function $F(Q;t,t_w)=\langle \rho(Q,t)\rho^*(Q,t_w)\rangle$, where the density fluctuations, $\rho(Q,t)$, have been defined above. (We recall here that $\langle\ \rangle$ is an average over the initial conditions which amounts to 100 independent samples). In light scattering experiments in out-of-equilibrium conditions, information on the dynamics of the system is obtained by measuring the time autocorrelation function of the scattered intensity, $g_2(Q;t,t_w)=\langle I(t_w+t)I(t_w)\rangle$. In the single scattering approximation the time autocorrelation function of the scattered intensity and the intermediate scattering function are connected by the relation $F(Q;t,t_w) \propto \sqrt{g_2(Q;t,t_w)-1}$, where the proportionality factor depends on the detection setup.

We start our study of the dynamics of density fluctuations focusing on the incoherent (one-particle) part of the intermediate scattering function, $F_s(Q;t,t_w)$,

$$F_s(Q;t,t_w)=\frac{1}{M}\left\langle \sum_{i=1}^{M} e^{-i\mathbf{Q}\cdot[\mathbf{X}_i(t+t_w)-\mathbf{X}_i(t_w)]}\right\rangle. \tag{10}$$

We recall here that $\mathbf{X}_i$ can either refer to the center of mass of platelets i, in which case $M=N$, or site positions, in which case $M=61\times N$. As already detailed above, the smallest value of the wave vector accessible in the simulation is $Q_m=2\pi/L \simeq 0.055$ nm^{-1}. We have used a wave-vector resolution $\Delta Q=0.005$ nm^{-1} and, for each value of Q, a maximum of 200 Q vectors has been considered in the calculation of averages. We note that, although scattering experiments mainly probe the collective intermediate scattering function, we expect to grasp the main features of the long-time aging dynamics also from $F_s(Q;t,t_w)$. This choice is mainly due to the fact that one-particle dynamics is less affected by noise than collective dynamics and, therefore, statistics is more reliable in the former case.

The quantities calculated from the position of the interaction sites also contain a dynamic contribution coming from rotations of the platelets; therefore, we expect the relative correlation functions to relax on time scales shorter than the analogous quantities calculated from the centers of mass of the platelets. Indeed, this is what we observe. In Fig. 5 we show our results at $Q=0.40$ nm^{-1}, at the indicated values of the waiting time t_w, both for centers of mass (left panel) and interaction sites (right panel). In Fig. 6 we show the simulation results at fixed $t_w \simeq 3.5$ μs at the indicated values of Q. From these two figures it is evident that aging is fully active in the system. In particular, the slowing down of the dynamics is larger the longer the aging time, and a clear Q dependence of the relaxation is visible at constant t_w. In the following we give a more detailed description of the effect of the aging time on the above dynamics.

The most natural choice would be to fit the data to a particular model and, then, to study the dependence on Q and

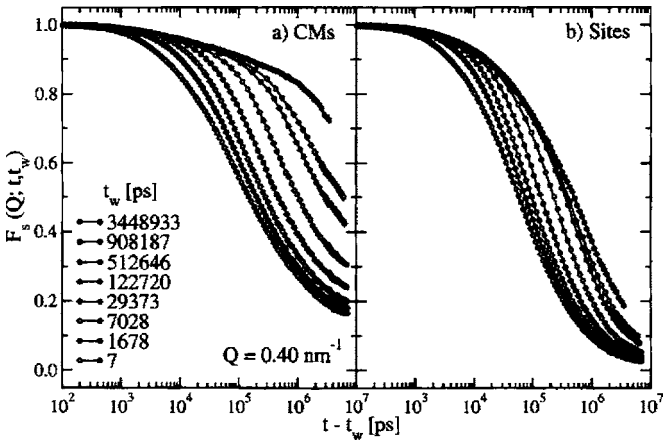

FIG. 5. t_w dependence of the incoherent (one-particle) intermediate scattering functions $F_s(Q;t,t_w)$ at $Q=0.40$ nm^{-1}, at the indicated values of t_w. (a) Data calculated from the positions of the platelet centers of mass. (b) Data calculated from sites, also containing orientational dynamics contributions. The effect of aging is evident from these data.

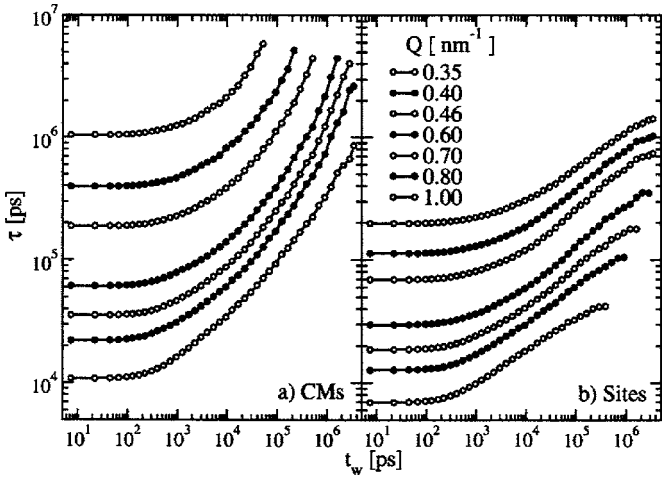

FIG. 7. Relaxation time for the incoherent intermediate scattering functions calculated by the threshold method with $f=e^{-1}$ for both centers of mass and sites as a function of the waiting time t_w. The indicated values of Q have been considered.

t_w of the fitting parameters. In doing so, we should take into account two important observations. First, we should note that most of the curves shown in Figs. 5 and 6 do not relax to zero on the available time window and this fact severely limits the possibility to fit the data without introducing arbitrary bounds. Second, in the present case t is always larger than or at most of the same order of magnitude of the waiting time t_w. This is in contrast to the case of experiments, where it is always $t_w \gg t$, and poses the question if it is reasonable to try to fit with a particular functional form a correlation function for times longer than the corresponding waiting time.

The above discussion amounts to identify a reasonable relaxation time scale for the intermediate scattering function which is independent of a particular model. We choose to use the method of the threshold we have described in the previous section in the case of the mean-squared displacement: we fix a particular threshold value and we consider as a relevant time scale the one at which the correlation function decreases from unity to the threshold value. Obviously, exploiting such a method we must take into account some caveats. Note, for instance, that the shape of the long-time relaxation (possibly representable by a stretched exponential) clearly changes with the waiting time and, therefore, the relaxation time alone is not the only relevant parameter. Nevertheless, we expect to understand the correct general behavior and also clarify the interplay between the aging time and the length scales actually relevant for the aging dynamics. *A posteriori* we also verify the above procedure in a particular case, fitting the data with a particular functional form and comparing the results.

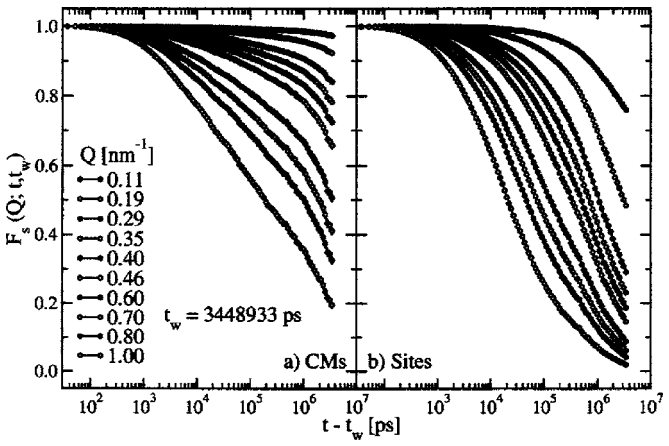

FIG. 6. Q dependence of the one-particle intermediate scattering function $F_s(Q;t,t_w)$ at $t_w=3\,448\,933$ ps at the indicated values of Q. (a) Data calculated on the platelet centers of mass. (b) Data calculated on interaction sites. A strong dependence on Q is evident from these data.

In Fig. 7 we show the results for both sites (left panel) and centers of mass (right panel) for a threshold value $f=e^{-1}$ as a function of the waiting time t_w, at the indicated values of Q. We have checked that the value chosen for the threshold does not qualitatively change the results. These data confirm the picture coming from the above analysis of the mean-squared displacement, pointing to a strong dependence of the out-of-equilibrium relaxation time on the waiting time. We observe that in our data the exponential dependence on the waiting time of the relaxation time visible at short waiting times in experiments is absent. (Note that the physical processes behind this particular feature in experiments still remain unexplained).[14]

To be more quantitative and to check the analysis introduced above, we fitted some of our data to a particular functional form, proposed some time ago and widely exploited in the literature (see, among others, Refs. 19–21 and 45). We choose, mainly due to a better quality of the data, the particular value $Q=0.7$ nm^{-1} and fit the curves to the following model:

$$F_s(Q;t,t_w) = f_Q(t_w)e^{-t/\tau_f(Q;t_w)} + (1-f_Q(t_w))e^{-(t/\tau_c(Q;t_w))^{\beta(Q;t_w)}}. \quad (11)$$

Here, we have introduced two relaxation times, i.e., τ_f, related to fast short-time dynamics, and τ_c, controlling the long-time relaxation. The nonergodicity parameter, $f_Q(t_w)$, and the stretching parameter, $\beta(Q;t_w)$, are reminiscent of the analogous quantities introduced for the study of the glass

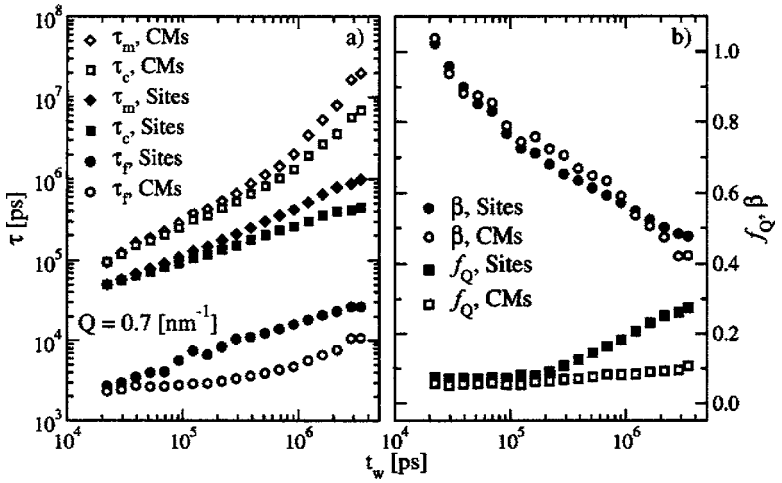

FIG. 8. Waiting time dependence of the parameters of the fit discussed in the text for the incoherent scattering function at $Q=0.7$ nm^{-1}.

transition. We fitted our data to Eq. (11) only for times tentatively shorter than $2t_w$. Figure 8 shows the t_w dependence of fitting parameters. The left panel shows τ_c, τ_f, and the "mean" relaxation time τ_m, defined as $\tau_m=\tau_c\Gamma(1/\beta)/\beta$, both for centers of mass of the platelets and interaction sites. All the data strongly depend on the waiting time and increase with t_w. The right panel shows our results for β, decreasing with t_w from 1 to about 0.4 (this behavior is also observed in experiments, see Ref. 45), and f_Q, which stays constant at a value of about 0.1 in the case of the center of mass and increases up to 0.3 for sites. Figure 9 shows the Q dependence of the same fitting parameters at constant $t_w \simeq 30$ ns. τ_f stays almost constant in the whole investigated Q range, while τ_c shows the typical Q^{-2} dependence.[24,46,47] Also, f_Q stays almost constant in the whole considered range (data for platelets and sites overlap almost perfectly), while β shows a slight decrease with Q in both cases.

We note that the above fits are particularly difficult due to the low statistics and to the fact that not all the curves relax to zero on the accessible time window. Moreover, the absence of a clear separation between time scales makes the determination of the relaxation times particularly difficult. More specifically, in some cases it was also possible to fit the data with two comparable values for τ_f and τ_c, obtaining a value of χ^2 comparable to the one of the actual fit with $\tau_f \ll \tau_c$.

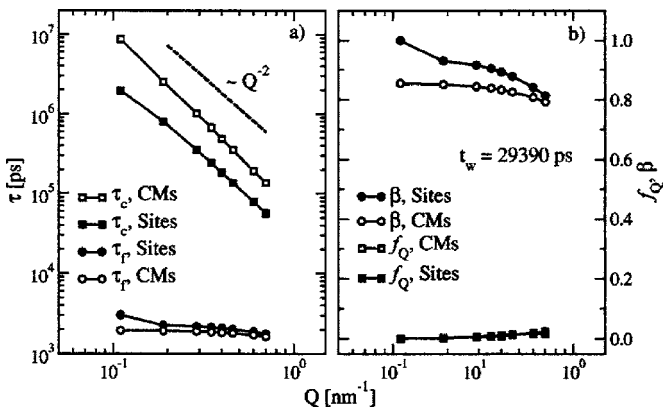

FIG. 9. Parameters of the fits discussed in the text for the incoherent scattering function at $t_w=29\,390$ ps as a function of the wave vector Q.

VIII. COLLECTIVE DYNAMICS OF DENSITY FLUCTUATIONS

The coherent intermediate scattering function at times t_w and t is defined as

$$F_c(Q;t,t_w)=\frac{1}{MS(Q)}\left\langle \sum_{i=1}^{M}\sum_{j=1}^{M} e^{-iQ\cdot[X_i(t+t_w)-X_j(t_w)]}\right\rangle, \qquad (12)$$

where X_i has been defined above and $S(Q)$ are the data included in Fig. 2. This function is related to the collective dynamics of the density fluctuations, and it is the quantity of direct relevance for the experimental measurements. In Fig. 10 we show the t_w dependence of $F_c(Q,t)$ at $Q=0.40$ nm^{-1}, both for centers of mass (left panel) and sites (right panel), while in Fig. 11 we show the Q dependence of $F_c(Q,t)$ at fixed $t_w \simeq 3.4$ μs, again for the two cases. Also these results confirm the strong t_w dependence of the out-of-equilibrium dynamics and do not seem to add much more insight to the analysis of the previous section. Indeed, the qualitative behavior of $F_c(Q;t,t_w)$ and $F_s(Q;t,t_w)$, as a function of both Q and t_w, is very similar, as is evident by comparing Fig. 10 to Fig. 5 and Fig. 11 to Fig. 6. Hence, the same conclusions of

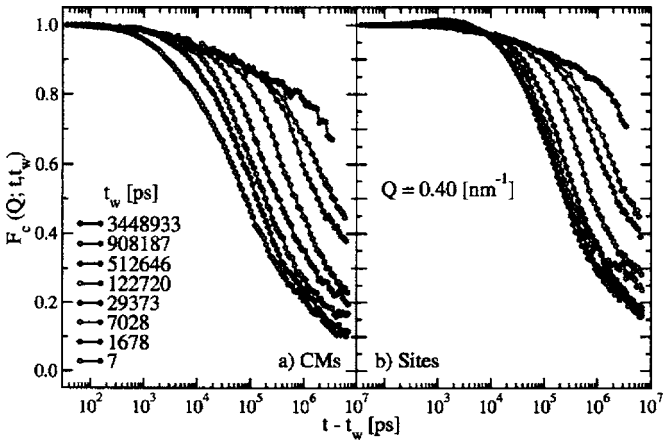

FIG. 10. t_w dependence of the coherent (collective) intermediate scattering function, $F_c(Q;t,t_w)$, at $Q=0.40$ nm^{-1}, at the indicated values of t_w (longer t_w's on top). Data calculated on the platelet centers of mass (a) and on interaction sites (b) are qualitatively in agreement.

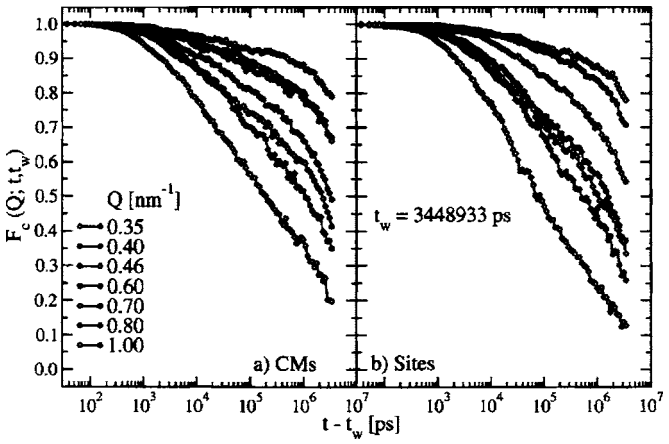

FIG. 11. Q dependence of the coherent intermediate scattering function, $F_c(Q;t,t_w)$, at $t_w=3\,448\,933$ ps at the indicated values of Q. Data calculated on the platelet centers of mass (a) and on interaction sites (b) show a qualitatively similar behavior.

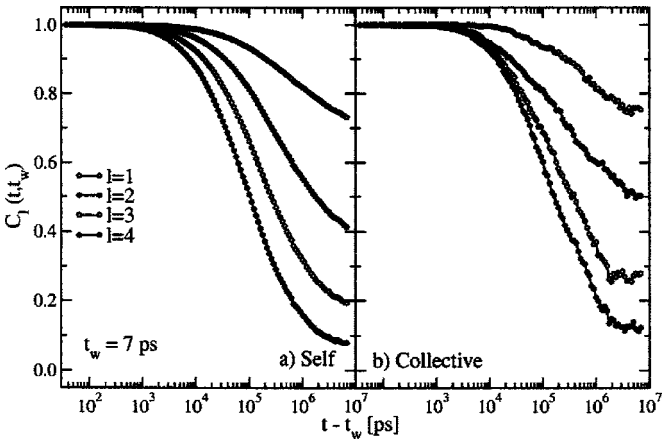

FIG. 13. Correlation functions of the Legendre polynomials of the order $1 \leqslant l \leqslant 4$ at $t_w \simeq 7$ ps. We show the self-contribution (left panel) and collective total case (right panel). The orientational relaxation dynamics is slower the higher the value of the order l.

Sec. VII can also be drawn from these results, at least at a qualitative level.

In the present case we do not attempt a direct fit of the data and directly exploit the method of the threshold to evaluate a reasonable relaxation time scale, independent of a particular functional form for a fitting model. Figure 12 shows our results, with a threshold $f=e^{-1}$, for the data at the indicated values of Q and as a function of the waiting time, t_w. Again, we have checked that the results do not qualitatively change with the chosen value of the threshold. Data are qualitatively in agreement with the results reported in Fig. 7 and confirm the overall picture we described in detail in the previous section.

IX. ROTATIONAL DYNAMICS

The strong anisotropy of the Laponite particle implies that an important role in dynamics and structural reorganization must be played by the mutual orientations of the platelets. Therefore, also from the above results, we expect that the orientational behavior of the system, both for the single platelet and collective, must strongly couple to the dynamics

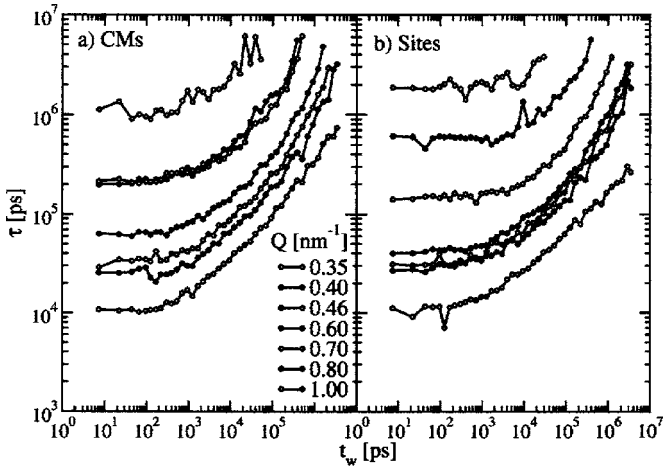

FIG. 12. Relaxation time for the coherent intermediate scattering functions calculated by the threshold method with $f=e^{-1}$ for centers of mass and sites as a function of the waiting time t_w at the indicated values of Q.

of density fluctuations and take place on comparable time scales. This is the main motivation for the present section.

The behavior of the orientational degrees of freedom is accessible via the dynamics of the Legendre polynomials calculated from the orientation vectors of platelets. Some of those polynomials are directly related to the response functions detected by different experimental techniques. The convenient correlation functions in this case are the functions $C_l(t,t_w)$ and their self-part $C_l^{(s)}(t,t_w)$, which are defined as

$$C_l(t,t_w)=\frac{1}{N}\left\langle \sum_{i=1}^{N}\sum_{j=1}^{N} P_l(\mathbf{u}_i(t+t_w)\cdot\mathbf{u}_j(t_w))\right\rangle, \tag{13a}$$

$$C_l^{(s)}(t,t_w)=\frac{1}{N}\left\langle \sum_{i=1}^{N} P_l(\mathbf{u}_i(t+t_w)\cdot\mathbf{u}_i(t_w))\right\rangle. \tag{13b}$$

Here, $\mathbf{u}_i$ is the normalized orientational vector of the ith particle, pointing along the normal to the surface of the platelet, and $P_l(x)$ is the Legendre polynomial of order l, with $l \geqslant 1$. Note that for $l=1$ and $l=2$, the functions $C_l(t)$ can be measured in dielectric and light scattering experiments. We also note that it is often assumed that the cross term in $C_l(t)$ can be neglected; in this case the experiments would also yield information on $C_l^{(s)}(t)$.

In Fig. 13 we show our results at $t_w=7$ ps at the indicated values of $1 \leqslant l \leqslant 4$, for the one-particle (left panel) and collective (right panel) cases, respectively. From these data it is evident that the smaller the value of l, the longer the time scale of the relaxation dynamics. In particular, note that in the collective case, the curves seem to saturate to a finite value at long time, pointing to a progressive freezing of the orientational degrees of freedom at very long times. Unfortunately the limited total time extension of the present computer simulation does not allow us to be conclusive on this point.

In Fig. 14 we plot our results for $l=2$ [panels (a) and (b)] and 4 [panels (c) and (d)] at the indicated waiting times, both for the self (left panels) and collective (right panels) cases. Again, also in the case of the rotational dynamics, a strong

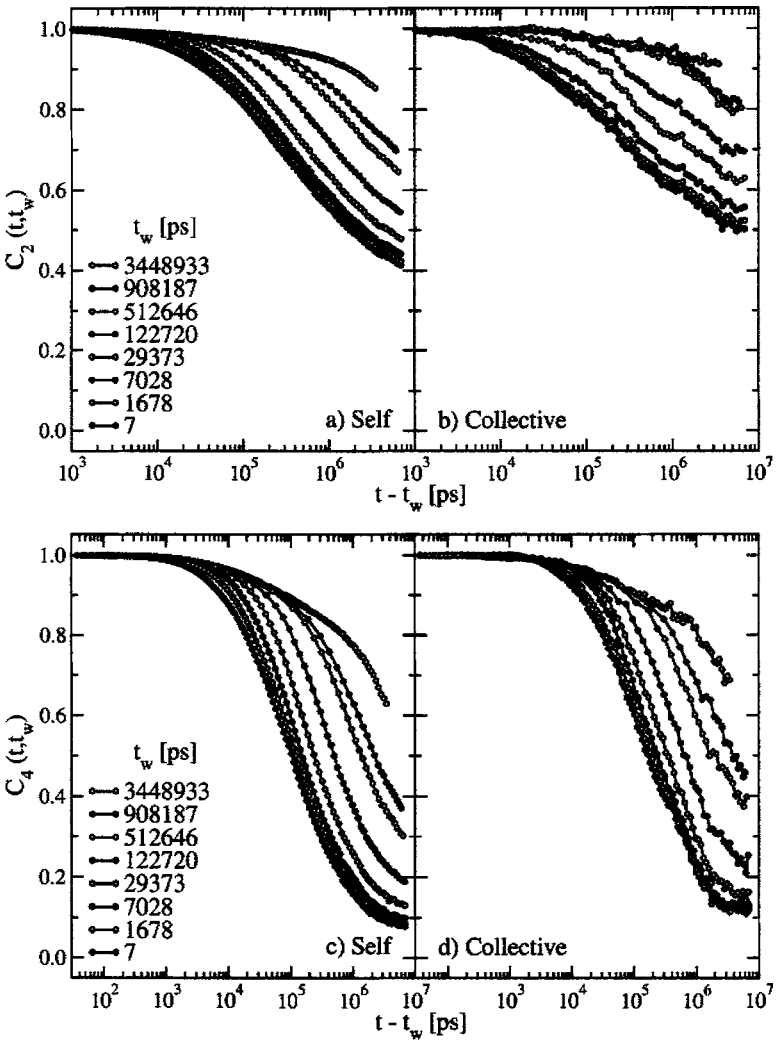

FIG. 14. Top: Waiting time dependence of the orientational correlation functions for $l=2$ (longer waiting times on the top), both for the self (left panel) and collective (right panel) cases. Bottom: Waiting time dependence of the orientational correlation functions for $l=4$ (shorter waiting times on the top) both for the self (left panel) and collective total cases (right panel).

aging time dependence is evident and at longer waiting times the rotational dynamics slows down significantly.

A threshold analysis similar to the one described above for the dynamics of density fluctuations allows one to identify a relaxation time. Our results are shown for $1 \leqslant l \leqslant 4$ in Fig. 15, where the threshold has been fixed to a value $f=0.8$. The overall qualitative behavior is analogous to the one found in the case of the translational dynamics, and the time scales, except for the case $l=1$, are also comparable in the two cases. Concluding, our data support a strong coupling between translational and orientational degrees of freedom,[48,49] as expected for a strongly anisotropic particle.

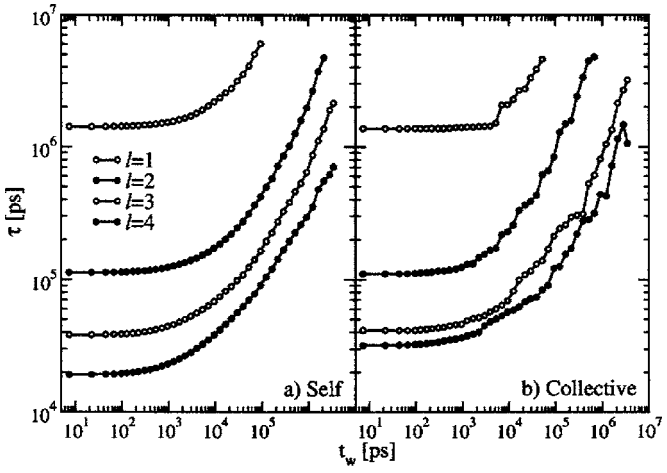

FIG. 15. Aging time dependence of the orientational relaxation time for the correlation functions of the Legendre polynomials of order $1 \leqslant l \leqslant 4$, determined by means of the threshold method, as discussed in the text. The threshold has been fixed to the value of $f=0.8$. Left panel: Data calculated from the self part of the correlation functions. Right panel: Data calculated from the total collective correlation functions.

X. CONCLUSIONS

In this work we have presented a systematic study of the out-of-equilibrium and aging dynamics of a model for a Laponite colloidal suspension. The choice of the system considered has been mainly suggested by the terrific amount of experimental work already present in the literature. A site-site, purely repulsive Yukawa-type interaction potential between Laponite platelets has been considered. We have used the Brownian dynamics technique for extensive molecular dynamics simulations. In particular, we have proposed a new algorithm which, although neglecting hydrodynamic effects, correctly takes into account the strong anisotropy of the Laponite platelet, introducing two different friction coefficients, respectively parallel and perpendicular to the direction of the symmetry axis of the platelet.

An extensive ensemble of independent systems has been driven out of equilibrium by an instantaneous jump from a high temperature to room temperature at constant volume fraction, and realistic configurations have been stored for the analysis. In particular, we have focused on the long-time aging dynamics, calculating the mean-squared displacement and the intermediate scattering functions. Both coherent and incoherent dynamics have been studied in detail. The dynamics of the density fluctuations has been found to be strongly dependent on the aging time, and a qualitative discussion has been performed on the interplay between the different time and length scales which play a significant role in the relaxation. A study of the rotational dynamics has completed the study of the dynamics of the Laponite colloidal suspension. The main result is that aging dynamics also strongly affects the orientational degrees of freedom, which relax on time scales comparable to the ones typical of translational modes.

The study presented here strongly suggests that, indeed, in the absence of attractive interactions between particles, a disordered arrested state can be generated only by the presence of Yukawa repulsive interactions. The long range of the repulsive interaction makes it possible to arrest the dynamics of the colloidal suspension even if the effective packing fraction is only a few percent. In this respect, cages are defined not by the physical size of the hard core but by the effective range of the screened electrostatic potential. While in the case of spherical particles, Yukawa interactions alone hardly generate a glass; due to the fast rates of crystallization induced by the long range of the interaction, the anisotropy of the platelets appears to be able to self-generate a sufficient local disorder which stabilizes the metastability of the arrested disordered state.

In this respect, despite the fact that our data are not conclusive, due to the difficulty of extending the time length of the simulation, charged platelets may give rise to Wigner glasses. Future work, in line with the present approach, must focus on the role played in the dynamics by both the salt concentration and the presence of opposite sign rim charges.

[1] F. Sciortino and P. Tartaglia, Adv. Phys. **54**, 471 (2005).
[2] L. Cipelletti and L. Ramos, J. Phys.: Condens. Matter **17**, R253 (2005).
[3] R. A. L. Jones, *Soft Condensed Matter* (Oxford University Press, Oxford, 2002).
[4] C. N. Likos, Phys. Rep. **348**, 267 (2001).
[5] D. Pontoni, T. Narayanan, J.-M. Petit, G. Grübel, and D. Beysens, Phys. Rev. Lett. **90**, 188301 (2003).
[6] T. Narayanan, M. Sztucki, G. Belina, and F. Pignon, Phys. Rev. Lett. **96**, 258301 (2006).
[7] R. E. Courtland and E. R. Weeks, J. Phys.: Condens. Matter **15**, S359 (2003).
[8] H. Tanaka and T. Araki, Phys. Rev. Lett. **85**, 1338 (2000).
[9] M. E. Cates, K. Stratford, R. Adhikari, P. Stansell, J.-C. Desplat, I. Pagonabarraga, and A. J. Wagner, J. Phys.: Condens. Matter **16**, S3903 (2004).
[10] J. Horbach and S. Succi, Phys. Rev. Lett. **96**, 224503 (2006).
[11] D. Bonn, H. Tanaka, G. Wegdam, H. Kellay, and J. Meunier, Europhys. Lett. **45**, 52 (1998).
[12] D. Bonn, S. Tomase, B. Abou, H. Tanaka, and J. Meunier, Phys. Rev. Lett. **89**, 015701 (2002).
[13] H. Tanaka, J. Meunier, and D. Bonn, Phys. Rev. E **69**, 031404 (2004).
[14] H. Tanaka, S. J. Farouji, J. Meunier, and D. Bonn, Phys. Rev. E **71**, 021402 (2005).
[15] T. Nicolai and S. Cocard, Langmuir **16**, 8189 (2000).
[16] T. Nicolai and S. Cocard, Eur. Phys. J. E **5**, 221 (2001).
[17] P. Mongondry, J. F. Tassin, and T. Nicolai, J. Colloid Interface Sci. **283**, 397 (2005).
[18] A. Mourchid, A. Delville, J. Lambard, E. Lécolier, and P. Levitz, Langmuir **11**, 1942 (1995).
[19] B. Ruzicka, L. Zulian, and G. Ruocco, Phys. Rev. Lett. **93**, 258301 (2004).
[20] B. Ruzicka, L. Zulian, and G. Ruocco, J. Phys.: Condens. Matter **16**, S4993 (2004).
[21] B. Ruzicka, L. Zulian, and G. Ruocco, Langmuir **22**, 1106 (2006).
[22] D. Bonn, H. Kellay, H. Tanaka, G. Wegdam, and J. Meunier, Langmuir **15**, 7534 (1999).
[23] F. Schosseler, S. Kaloun, M. Skouri, and J. P. Munch, Phys. Rev. E **73**, 021401 (2006).
[24] M. Bellour, A. Knaebel, J. L. Harden, F. Lequeux, and J.-P. Munch, Phys. Rev. E **67**, 031405 (2003).
[25] L. Cipelletti, S. Manley, R. C. Ball, and D. A. Weitz, Phys. Rev. Lett. **84**, 2275 (2000).
[26] S. Kaloun, M. Skouri, A. Knaebel, J.-P. Münch, and P. Hébraud, Phys. Rev. E **72**, 011401 (2005).
[27] S. Kutter, J.-P. Hansen, M. Sprik, and E. Boek, J. Chem. Phys. **112**, 311 (2000).
[28] M. Dijkstra, J.-P. Hansen, and P. A. Madden, Phys. Rev. E **55**, 3044 (1997).
[29] E. Trizac, L. Bocquet, R. Agra, J.-J. Weis, and M. Aubouy, J. Phys.: Condens. Matter **14**, 9339 (2002).
[30] G. Odriozola, M. Romero-Bastida, and F. de J. Guevara-Rodriguez, Phys. Rev. E **70**, 021405 (2004).
[31] F. Sciortino, S. Mossa, E. Zaccarelli, and P. Tartaglia, Phys. Rev. Lett. **93**, 055701 (2004).
[32] S. Mossa, F. Sciortino, P. Tartaglia, and E. Zaccarelli, Langmuir **20**, 10756 (2004).
[33] L. Li, L. Harnau, S. Rosenfeldt, and M. Ballauff, Phys. Rev. E **72**, 051504 (2005).
[34] S. Mossa, C. De Michele, and F. Sciortino (unpublished).
[35] G. Ciccotti, M. Ferrario, and J.-P. Ryckaert, Mol. Phys. **47**, 1253 (1982).
[36] E. J. W. Verwey and J. T. G. Overbeek, *Theory of Stability of Lyophobic Colloids* (Elsevier, Amsterdam, 1948).
[37] D. L. Ermak and J. A. McCammon, J. Chem. Phys. **69**, 1352 (1978).
[38] W. F. van Gunsteren and H. J. C. Berendsen, Mol. Phys. **45**, 637 (1982).
[39] M. P. Allen and D. J. Tildesley, *Computer Simulation of Liquids*, 2nd ed. (Clarendon, Oxford, 1989).
[40] A. Mourchid, E. Lécolier, H. V. Damme, and P. Levitz, Langmuir **14**, 4718 (1998).
[41] S. C. McGrother, D. C. Williamson, and G. Jackson, J. Chem. Phys. **104**, 6755 (1996).
[42] H. Shimizu, J. Chem. Phys. **37**, 765 (1962).
[43] J.-P. Bouchaud, J. Phys. I **2**, 1705 (1992).
[44] J.-P. Bouchaud, in *Soft and Fragile Matter*, edited by M. E. Cates and M. R. Evans (IOP, London, 2000).
[45] B. Abou, D. Bonn, and J. Meunier, Phys. Rev. E **64**, 021510 (2001).
[46] F. Schosseler, S. Jaloun, M. Skouri, and J. P. Munch, Phys. Rev. E **73**, 021401 (2006).
[47] L. Cipelletti, L. Ramos, S. Manley, E. Pitard, D. A. Weitz, E. E. Pashkovski, and M. Johansson, Faraday Discuss. **123**, 237 (2003).
[48] S. Jabbari-Rarouji, E. Eiser, G. H. Wegdam, and D. Bonn, J. Phys.: Condens. Matter **16**, L471 (2004).
[49] L. Fabbian, F. Sciortino, and P. Tartaglia, J. Non-Cryst. Solids **235–237**, 325 (1998).
[50] S. Kaloun, R. Skouri, M. Skouri, J.-P. Münch, and F. Schosseler, Phys. Rev. E **72**, 011403 (2005).